Preoperative [18F]fluoro-PEG-folate PET/CT in advanced stage epithelial ovarian cancer: a safety and feasibility study

Ciggaar, I.A.; Muynck, L.D.A.N. de; Geus-Oei, L.F. de; Velden, F.H.P. van; Kroon, C.D. de; Arias-Bouda, L.M.P.; ... ; Gaarenstroom, K.N.

Nuclear Medicine and Biology 138-139 (2024) 108952

Contents lists available at ScienceDirect

Nuclear Medicine and Biology

journal homepage: www.elsevier.com/locate/nucmedbio

Preoperative [^{18}F]fluoro-PEG-folate PET/CT in advanced stage epithelial ovarian cancer: A safety and feasibility study

Isabeau A. Ciggaar [a,1], Lysanne D.A.N. de Muynck [b,1], Lioe-Fee de Geus-Oei [a], Floris H.P. van Velden [a], Cornelis D. de Kroon [c], Lenka M. Pereira Arias-Bouda [a], Wyanne A. Noortman [a], Els L. van Persijn van Meerten [d], Petra Dibbets-Schneider [a], Hendrik J.F. Helmerhorst [e], Albert D. Windhorst [f], Alexander L. Vahrmeijer [b], Inge T.A. Peters [c,1], Katja N. Gaarenstroom [c,*,1]

[a] Department of Radiology, Section of Nuclear Medicine, Leiden University Medical Center, Leiden, the Netherlands
[b] Department of Surgery, Leiden University Medical Center, Leiden, the Netherlands
[c] Department of Gynecology, Leiden University Medical Center, Leiden, the Netherlands
[d] Department of Radiology, Leiden University Medical Center, Leiden, the Netherlands
[e] Department of Anesthesiology and Intensive Care, Leiden University Medical Center, Leiden, the Netherlands
[f] Department of Radiology, Amsterdam UMC, Location AMC, Amsterdam, the Netherlands

ARTICLE INFO

Keywords:
Epithelial ovarian cancer
Cytoreductive surgery
PET/CT
Folate receptor
Molecular imaging

ABSTRACT

Purpose: The selection for either primary or interval cytoreductive surgery (CRS) in patients with epithelial ovarian cancer (EOC) is currently based on imaging techniques like computed tomography (CT), [^{18}F]fluorodeoxyglucose-positron emission tomography ([^{18}F]FDG-PET), diffusion-weighted magnetic resonance imaging (DW-MRI) and/or diagnostic laparoscopy, but these have limitations. Folate receptor (FR)-targeted PET/CT imaging, using [^{18}F]fluoro-PEG-folate, could improve preoperative assessment, potentially reducing unnecessary laparotomies. This paper presents the first experience with [^{18}F]fluoro-PEG-folate PET/CT imaging in advanced stage EOC, focusing on safety, tolerability, and feasibility for reflecting the extent of disease.

Methods: Tolerability and safety were monitored after administration of the [^{18}F]fluoro-PEG-folate tracer by measurements of vital function parameters (blood pressure, heart rate, peripheral oxygen saturation, respiratory rate, and temperature). In addition, (serious) adverse events were recorded. Disease burden was quantified using the Peritoneal Cancer Index (PCI) score on preoperative [^{18}F]fluoro-PEG-folate PET/CT and during surgery. PCI scores were compared with intraoperative findings, considering histopathologic results as the gold standard. Tissue specimens were stained for FRα and FRβ. Relative uptake of the radiotracer by EOC lesions and other tissues was quantified using body weighted standardized uptake values (SUV).

Results: The study was terminated prematurely during the interim analysis after inclusion of eight patients of whom five had completed the study protocol. Although [^{18}F]fluoro-PEG-folate demonstrated safety, efficacy for tumor-specific imaging was limited. Despite clear FRα overexpression, low tracer uptake was observed in EOC lesions, contrasting with high uptake in healthy tissues, posing challenges in specificity and accurately assessing tumor burden.

Conclusions: Overall, while [^{18}F]fluoro-PEG-folate was well-tolerated, its clinical utility in the preoperative assessment of the extent of disease in EOC was limited. This highlights the need for further research in developing targeted imaging agents for optimal detection of EOC metastases.

Trial registration: Clinicaltrials.gov, NCT05215496. Registered 31 January 2022.

* Corresponding author at: Postbus 9600, 2300 RC, Leiden, the Netherlands.
E-mail address: k.n.gaarenstroom@lumc.nl (K.N. Gaarenstroom).
[1] These authors contributed equally to this work.

https://doi.org/10.1016/j.nucmedbio.2024.108952
Received 24 July 2024; Received in revised form 13 September 2024; Accepted 17 September 2024
Available online 19 September 2024

1. Introduction

Epithelial ovarian cancer (EOC) is the leading cause of death from gynecological cancer in developed countries. Approximately 75 % of women are diagnosed with advanced disease (FIGO stage III-IV) [1]. The standard approach for treatment with curative intent involves a combination of cytoreductive surgery (CRS) and platinum-based chemotherapy, usually with carboplatin and paclitaxel [2]. Whether neoadjuvant chemotherapy (NACT) is administered prior to CRS depends on the extent of disease at initial diagnosis and surgical resectability, as well as performance status and co-morbidity [2]. Completeness of CRS is the most significant prognostic variable for survival in advanced stage disease. In cases where complete cytoreduction seems feasible, upfront CRS is standard of care [2–4].

Preoperative assessment of resectability is commonly determined via computed tomography (CT). However, the reported accuracy of CT for peritoneal implantation detection ranges from 25 to 90 % [5,6]. Smaller lesions are known limitations of CT imaging, with a lowered sensitivity of 9 to 50 % for lesions <1 cm, and only 11 % for nodules <0.5 cm [6]. As a result, the extent of peritoneal carcinomatosis is often underestimated by CT. This can label patients as operable and may result in an unnecessary laparotomy [2,7,8]. Fagotti et al. described that a laparoscopy-based score can reliably predict the chance of optimal cytoreduction in advanced EOC [9,10]. Furthermore, Rutten et al. demonstrated in a randomized study that performing a diagnostic laparoscopy before CRS in advanced stage EOC patients reduced the rate of unnecessary laparotomies from 39 % to 10 % [11]. However, while laparoscopy can be a valuable tool for identifying patients who are likely to achieve complete CRS, it remains an invasive procedure and its effectiveness can be limited in cases with bulky tumors and adhesions [12,13].

Other promising imaging modalities to detect peritoneal metastases include positron emission tomography (PET), most commonly with [^{18}F]fluorodeoxyglucose ([^{18}F]FDG-PET), and diffusion-weighted magnetic resonance imaging (DW-MRI) [6,14,15]. However, the accuracy of [^{18}F]FDG-PET is limited because of the heterogeneous metabolic activity seen in EOC tissue, which can result in decreased sensitivity. Although DW-MRI showed a significantly higher accuracy than CT for primary tumor characterization, staging and prediction of incomplete resection [6,14,15], whole-body DW-MRI underestimated inoperable diffuse carcinomatosis of the small bowel in recurrent EOC [6,15]. In addition, the diagnostic accuracy of DW-MRI to differentiate between healthy and pathological lymph nodes seems limited since both showed diffusion restriction [16].

The use of a tumor-targeted PET tracer could allow for greater sensitivity and specificity in detecting lesions. Tumor-targeted imaging shows promise in accurately assessing disease extent by specifically targeting tumor cells or their microenvironment [17]. Integrating this approach into preoperative evaluations could significantly improve identification of irresectable disease and guide treatment decisions more effectively.

Folate receptors (FRs) are overexpressed in 90–95 % of EOC cells and are promising targets for tumor-targeted imaging of EOC [18–21]. Studies with OTL-38, a folate analogue conjugated to a near-infrared (NIR) fluorophore, have shown specific accumulation in EOC metastases with a high tumor-to-background ratio. Intraoperative imaging with OTL-38 in advanced-stage EOC patients identified 29–33 % additional malignant lesions that were otherwise not visible with the naked eye [22,23]. Similarly, the use of FR-targeted PET imaging has been explored in ovarian cancer mouse models [24–26]. After intravenous tail injection of 4–11 MBq of folate-PEG12–NOTA-AI^{18}F in mice bearing FR-positive xenografts, tumors were clearly visible on a microPET scan. Uptake of folate-PEG12–NOTA-AI^{18}F was blocked when 50 μg of folic acid was administered prior to radiotracer infusion, indicating a highly specific uptake mediated by FR [26]. A similar FR-targeted PET tracer, [^{18}F]fluoro-PEG-folate, has demonstrated its safety, tolerability and feasibility in 22 patients with rheumatoid arthritis [27]. Given its high affinity for FR-positive cells, [^{18}F]fluoro-PEG-folate seems suited for the detection of metastatic lesions by tumor-targeted PET imaging in EOC.

In the present study, we aimed to evaluate the safety, tolerability, and efficacy of [^{18}F]fluoro-PEG-folate PET/CT imaging in advanced stage IIIB/IIIC EOC. The pharmacokinetics of [^{18}F]fluoro-PEG-folate have been described separately by Ruytenberg et al. [28].

2. Materials and methods

This phase I study in patients with advanced stage EOC was centrally approved by the Medical Ethics Committee Leiden-Den Haag-Delft (protocol P20.048, Clinicaltrials.gov: NCT05215496). The intention was to include 15 patients in this pilot. Informed consent was obtained from all individual participants included in the study. The primary objective was to evaluate the safety, tolerability, and pharmacokinetics of [^{18}F]fluoro-PEG-folate. The secondary objective was to assess the feasibility of a [^{18}F]fluoro-PEG-folate PET/CT scan for preoperative detection of intra-abdominal metastatic EOC lesions.

2.1. Patient selection

Patients who presented at the Department of Gynecology, Leiden University Medical Center (LUMC), The Netherlands, between September 2021 until October 2022 with advanced stage EOC and were scheduled for either primary or interval CRS, were asked to participate in the study. The following inclusion criteria were set: FIGO stage IIIB/IIIC EOC based on conventional CT scan; histologically proven EOC, or cytologically suspected EOC in combination with a serum CA125/CEA ratio > 25; above 30 years of age, able to comply with the study procedures and provide written informed consent. The exclusion criteria were: pregnancy; lactation; severe claustrophobia; thrombocytopenia (platelet count $<100 \times 10^9$/L) and/or INR > 2; impaired renal function (defined as eGFR <50 mL/1.73 m^2); impaired liver function (ALT, AST or total bilirubin >3× upper limit of normal); clinically significant abnormalities on electrocardiography (ECG); inability to tolerate lying supine for the duration of a PET/CT examination (~110 min), and concomitant malignancy (except basal cell carcinoma of the skin).

All patients underwent a standard CT scan of the chest and abdomen with intravenous iodine contrast (portal venous phase). Patients were selected for either upfront or interval CRS according to co-morbidity, and the extent of metastatic disease and presumed feasibility of complete cytoreduction as assessed by CT scan [2,4].

2.2. FR-targeted PET scan

[^{18}F]fluoro-PEG-folate was synthesized individually for each patient under GMP conditions by the Department of Radiology and Nuclear Medicine at Amsterdam UMC, location VUmc, the Netherlands. The PET/CT scans were performed within 3 weeks but at least 24 h before CRS. Participants were asked to not use any folate containing medication or supplements (vitamin B9/B11 or folic acid) for at least 7 days before the PET/CT scan. Prior to the scan, an arterial catheter was inserted into the participants' radial artery to collect blood samples for pharmacokinetic analysis. A dose of 185 MBq [^{18}F]fluoro-PEG-folate was administered intravenously by automatic bolus injection. Immediately post-injection, a dynamic PET-CT scan was performed of the pelvic region for 90 min with an integrated digital PET/CT scanner (Vereos, Philips Healthcare, Best, The Netherlands) to perform pharmacokinetic modelling [28]. After a short break to provide some comfort to the patient, an extra low-dose CT scan (50 mA eff, 120 kV) and a static PET scan (5 min/bed position) was made of the abdomen for anatomical correlation with abnormalities on the PET/CT. Image data was reconstructed according to EARL ^{18}F standard 1 (OSEM with 3 iterations, 15 subsets, 5.5 mm full-width-at-half-maximum Gaussian smoothing). The relative uptake of the radiotracer by EOC lesions and other tissues was

quantified using body weighted standardized uptake values (SUV).

2.3. Safety monitoring

Tolerability assessments (blood pressure (mmHg), pulse rate (bpm), peripheral oxygen saturation, respiratory rate, and temperature) were performed every 15 min starting directly before administration and continued up to 120 min after the administration of [^{18}F]fluoro-PEG-folate. An ECG was acquired directly after the PET/CT scan and patients were observed by a physician up to 2 h after administration. Additionally, (serious) adverse events and the concomitant use of other medications were recorded until six weeks after the administration of [^{18}F]fluoro-PEG-folate.

2.4. Evaluation of disease extent

Metastatic disease burden was assessed and quantified on the static [^{18}F]fluoro-PEG-folate PET/CT images (~90 min p.i.) and during surgery by using the peritoneal cancer index (PCI) score [29]. The PCI was used to quantify the extent of metastatic spread in 13 abdominal regions. Each region received a score based on the amount of tumor involvement: 0 for no macroscopic tumor, 1 for small (<0.5 cm), 2 for moderate (0.5–5.0 cm) and 3 for large tumor lesions (>5 cm) [29]. Scores for each region were added to obtain a total PCI. Morphologically suspect or enlarged (size ≥1 cm) pelvic or paraaortic lymph nodes were also noted and measured.

PCI scores were obtained from the static [^{18}F]fluoro-PEG-folate PET/CT images ($PCI_{PET/CT}$) via consensus reading by two experienced nuclear medicine physicians (LGO, LP). The PCI during surgery ($PCI_{surgery1}$) was determined by the operating gynecologic oncologist, blinded to the result of the PET/CT, during initial exploratory laparotomy. Following this, the result of the PET/CT was presented to the surgeon, allowing for a 'second look' i.e., secondary assessment of the surgical PCI ($PCI_{surgery2}$). Alongside the PCI scores, in which only the largest lesion contributes to the score per region, a list of all tumor lesions suspected of malignancy was provided by PET/CT and surgery. According to standard care, lesions considered malignant were excised during CRS when surgically feasible. Preoperative findings on PET/CT were compared with the intraoperative findings based on the PCI scores, considering histopathologic results as gold standard.

2.5. Pathology and immunohistochemistry

Whole formalin-fixed paraffin-embedded (FFPE) tissue blocks of lesions removed during CRS were cut into sections of 4 μm thickness. Sections were deparaffinized in xylene and rehydrated in a stepwise series of alcohol solutions. Given that FRα is the predominant isoform expressed in tumor tissue, staining for FRα was performed on all the resected and/or biopsied tissue specimens using an immunohistochemical assay kit according to the manufacturer's instructions (26B3.F2, BioCare Medical, USA). After being rinsed in PBS, the immunoreactions were visualized using DAB substrate buffer (Dako, Denmark) for 10 min and counterstained using Mayer's hematoxylin for 15 s. After dehydration at 37 °C, the stained slides were mounted with Pertex (Leica Microsystems, Germany). Hematoxylin and eosin (H&E) stainings were also made of each FFPE block.

Due to the identification of FRβ in false positive lymph nodes in prior studies [23], we conducted immunohistochemical staining for FRβ on the false positive lesions identified on the static [^{18}F]fluoro-PEG-folate PET/CT images. After deparaffinization and rehydration, endogenous peroxidase activity was blocked with 0.3 % hydrogen peroxide for 20 min. FRβ epitopes were unmasked by heat induction at 95 °C using Tris/EDTA buffer (pH 9.0, Dako, Glostrup, Denmark) in a PT-Link module (Agilent, Santa Clara, CA, USA). The slides were then incubated overnight in a humidified chamber at room temperature with a primary monoclonal antibody against FRβ (1/150, Invitrogen MA5-26933). The slides were washed in PBS thrice and incubated for 30 min at room temperature with a horseradish peroxidase (HRP)-labelled anti-rabbit secondary antibody (Envision, Dako). Slides were rinsed in PBS and immunoreactions were visualized, counterstained and coverslipped as described above.

All immunohistochemically stained slides were digitalized using the Panoramic Digital Slide Scanner and viewed with CaseViewer 2.6 (3D Histech, Hungary). Staining in tumor tissue was evaluated using the total immunostaining (TIS) score based on membranous expression. The TIS score consists of the total amount of positively stained tumor cells as a percentage of total tumor tissue (proportion score [PS]; 0 ≤ 10 %, 1 = 10–25 %, 2 = 26–50 %, 3 = 51–75 %, 4≥ 75 %), and the staining intensity (intensity score [IS]; 0 = none, 1 = weak, 2 = moderate, 3 = strong). These scores are then multiplied (PS × IS) to give a final TIS score of one of nine possible values: 0 = no expression, 1–4 = weak expression, 6, 8 = moderate expression, 9, 12 = strong expression [20].

3. Results

3.1. Study subjects

Out of 62 patients screened for the study between September 2021 and October 2022, eight patients were included. Besides meeting the exclusion criteria, the primary reasons for nonparticipation were patients assessing themselves as being in poor condition after NACT, the intensive nature of the study protocol, insufficient residual disease post-NACT (i.e., no lesions left that were suitable for pharmacokinetic modelling ≥1.5 cm), and logistical challenges in scheduling the scan and surgery within the intended timeframe (≤3 weeks). Three patients were unable to undergo the [^{18}F]fluoro-PEG-folate PET/CT acquisition after inclusion due to failed tracer productions that did not meet release criteria (radiochemical purity ≥95 %). The specifications of the tracer production of the five patients who underwent [^{18}F]fluoro-PEG-folate PET/CT imaging, such as radiochemical yield, purity, and molar activity are shown in Supplementary Table 1. Supplementary Fig. 1 shows the HPLC chromatogram of a representative [^{18}F]fluoro-PEG-Folate sample from one patient, demonstrating the purity and peak distribution. The study was concluded prematurely due to unsatisfactory interim analysis results regarding feasibility when only five participants, out of the initially planned 15 participants, had successfully completed the study protocol with PET/CT imaging.

All five patients were preoperatively diagnosed with FIGO stage IIIC high grade serous ovarian cancer via preoperative CT scans and histological examination of omental biopsies. Their median age was 67 years (range: 44–71 years). One patient underwent primary CRS, while four patients received 3–4 courses of NACT (paclitaxel 175 mg/m^2 and carboplatin AUC 5–6 mg/mL/min) before the [^{18}F]fluoro-PEG-folate PET/CT scan and interval CRS. Two patients who underwent interval CRS also underwent intra-abdominal lavage with hyperthermic chemotherapy (HIPEC) involving the administration of cisplatin (100 mg/m^2) after completing cytoreduction [30]. The time interval between the [^{18}F]fluoro-PEG-folate PET/CT acquisition and surgery ranged from 3 to 21 days. None of the patients received NACT between the PET/CT scan and CRS. In all patients a complete CRS was reached without macroscopically residual tumor.

3.2. Safety and tolerability

No serious adverse events (SAE) occurred during this study. No relevant changes in the parameters of the tolerability assessments were observed up to 120 min after the administration of [^{18}F]fluoro-PEG-folate (Supplementary Table 2). There were no abnormalities on the ECGs that were acquired directly after the PET/CT scan and no clinical abnormalities during the 120 min observation by a physician post administration of the radiotracer.

3.3. [^{18}F]fluoro-PEG-folate PET/CT images

Visual inspection revealed a pattern of tracer accumulation on all the static [^{18}F]fluoro-PEG-folate PET/CT images. High and slightly irregular tracer accumulation was observed in the liver and spleen, and high accumulation in the gallbladder and biliary system, stomach, duodenum, pancreas, adrenal glands renal cortices, renal pelvis, ureters, bone marrow, and bowel. Moderate tracer accumulation was observed in the bladder and numerous (reactive) lymph nodes. Residual activity was observed in the descending aorta. In Fig. 1, the maximum intensity projections (MIP) images of the scan illustrate this distribution.

To put the relative uptake in various organs and/or structures into perspective, Table 1 presents the mean SUV_{max} (g/mL) measurements of the most intense EOC lesions (15 lesions in five patients), the respective adjacent bowel wall, general blood pool (measured in the descending aorta) and liver.

The majority of EOC lesions were difficult to differentiate due to their low tracer uptake, small size and close proximity to other organs or structures with high tracer accumulation (such as bowel and vessels). As shown in Table 1, the mean SUV of the bowel wall and lymph nodes was comparable to the SUV of the tumor lesions. The mean SUV of the liver was even higher, making it challenging to identify any tumor deposits located at the Glisson's liver capsule. Additionally, peritoneal metastatic disease often presented as (confluent) miliary nodules and/or fat infiltration, appearing as an indistinct hazy area with low tracer uptake (Fig. 1, scan A). Furthermore, uptake of [^{18}F]fluoro-PEG-folate was also observed in tumor-negative lymph nodes (Fig. 1, scan B).

Fig. 2 shows a representative example of how a certain lesion was correlated on a diagnostic (contrast enhanced) CT image, [^{18}F]fluoro-PEG-folate PET/CT images, during surgery and by histopathological and immunohistochemical evaluation. Apart from the peritoneal lesion, high tracer accumulation was seen in the bowel wall and bone marrow.

3.4. Peritoneal cancer index (PCI) scores

Table 2 shows that the total $PCI_{PET/CT}$ was 1–2 points higher than $PCI_{surgery2}$ in all five patients. There was a discrepancy between the $PCI_{PET/CT}$ and $PCI_{surgery1}$ in 19 out of 65 abdominal regions, and in 17 out of 65 regions between $PCI_{PET/CT}$ and $PCI_{surgery2}$. In 18 of the 65 abdominal regions, the presence of malignant lesions was histologically confirmed. In two patients, miliary peritoneal lesions in six abdominal regions were vaporized without histopathologic confirmation, but comparable to other peritoneal lesions which were proven malignant in the same patient. In 11 out of the 18 abdominal regions with proven malignancy, the tumor positive lesions were both recognized on [^{18}F]fluoro-PEG-folate PET/CT images and during surgical exploration ($PCI_{surgery1}$ and $PCI_{surgery2}$).

In two patients, three additional tumor positive lesions in the central region and right flank were recognized during second surgical exploration based on folate-PET/CT findings. Among four patients, $PCI_{PET/CT}$ scores of $\geq$1 were observed in a total of nine abdominal regions where no tumor lesions were seen during surgery. In four patients, a total of five regions appeared tumor-negative on folate-PET/CT images but were considered tumor positive in both $PCI_{surgery1}$ and $PCI_{surgery2}$. Histopathological assessment confirmed three of these regions as tumor-positive, one as tumor-negative, and one region lacked a conclusive histopathological evaluation. Additionally, two regions, the omentum (central) and adnexa (pelvis), were deemed false-negative on $PCI_{PET/CT}$, $PCI_{surgery1}$ and $PCI_{surgery2}$. Following their removal according to standard surgical cytoreduction, histopathological assessment confirmed malignancy.

A total of 48 para-aortic, para-iliac, and inguinal lymph nodes showed radiotracer uptake on [^{18}F]fluoro-PEG-folate PET/CT images. Only one iliac lymph node out of the 48 PET-positive nodes was enlarged and suspected of malignancy during surgery and therefore removed. This node appeared to be a conglomerate of three tumor-negative lymph nodes on histopathology. The other 47 lymph nodes appeared non-suspicious or enlarged during surgery and were not removed according to the protocol.

3.5. Immunohistochemical analysis

All tumor-positive lesions showed positive FRα staining confirmed via immunohistochemistry (Table 3). Lesions from primary CRS all had a TIS between 9 and 12, while lesions from interval CRS had a slightly lower TIS. This corresponds with our previous study [20].

The conglomerate of three false-positive lymph nodes on PET/CT images that were removed was completely negative for tumor-

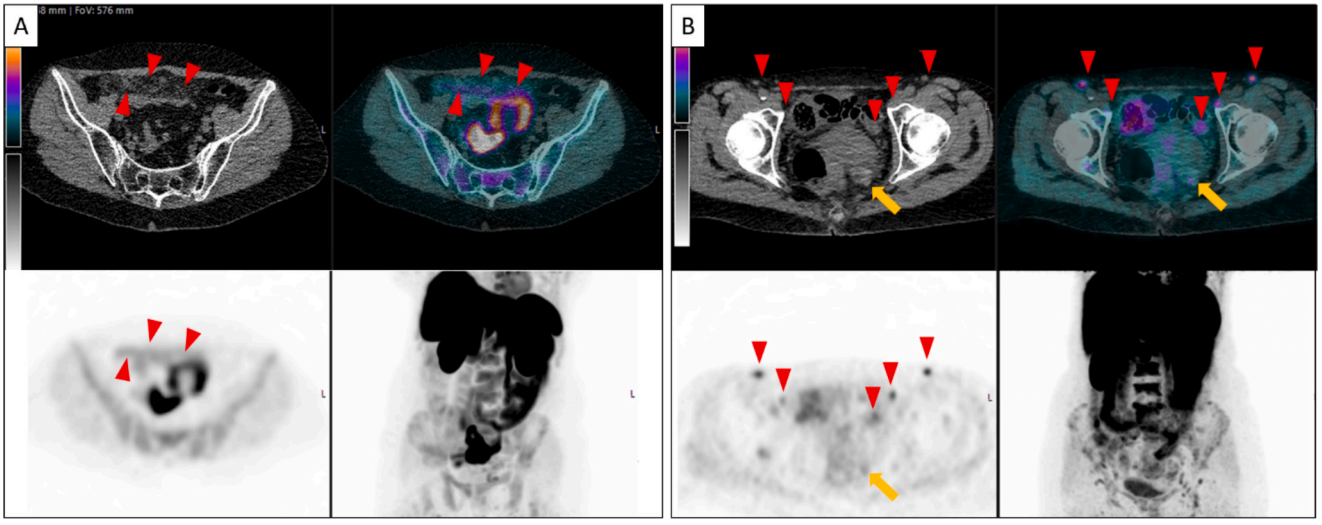

Fig. 1. [^{18}F]fluoro-PEG-folate PET/CT: low tracer uptake of EOC metastases (confluent tumor lesions in the omentum) and high uptake in numerous lymph nodes. Two [^{18}F]fluoro-PEG-folate PET/CT scans are presented within each image: a low-dose CT image (left upper corner), PET image (left lower corner), fused PET/CT image (right upper corner), and MIP images of the PET scan (right lower corner). **(A)** Left PET/CT scan: confluent metastatic disease in the omentum (red arrows) with low tracer accumulation and limited visibility, next to the bowel wall with intense bowel signal (mismatch between PET and CT images). **(B)** Right PET/CT scan: bilateral inguinal and pelvic nodes (red arrows) with high tracer accumulation. The primary EOC mass on the right behind the uterus (yellow arrows) shows almost no tracer accumulation and some calcifications on non-contrast enhanced CT).

Table 1
Measurements of tracer accumulation (mean SUV_{max}) on static [^{18}F]fluoro-PEG-folate PET/CT images (measured in EARL ^{18}F standard 1 reconstructions).

Patient	EOC lesions mean SUV_{max} (range)	Bowel wall mean SUV_{max} (range)	Lymph nodes mean SUV_{max} (range)	Liver SUV_{max}	Blood pool SUV_{max}
1	2.71 (2.58–2.80)	1.97 (1.59–2.26)	2.96 (2.65–3.22)	11.42	1.46
2	2.55 (1.32–3.23)	7.42 (2.26–10.20)	3.03 (2.11–3.56)	10.23	1.84
3	2.25 (1.59–2.70)	3.26 (3.23–3.28)	1.34 (1.18–1.58)	14.66	1.40
4	1.30 (0.92–1.80)	2.94 (1.35–6.03)	1.36 (1.07–1.71)	13.86	0.83
5	3.25 (2.54–3.79)	4.68 (3.91–6.08)	3.24 (2.88–3.59)	13.44	1.22

The mean SUVmax (g/mL) for EOC lesions, bowel wall and lymph nodes were calculated based on 3 measurements per patient (the three most intense EOC lesions and lymph nodes, and at three bowel wall sites). Activity in the blood pool was measured in the descending aorta; bowel was measured adjacent to the 15 respective EOC lesions.

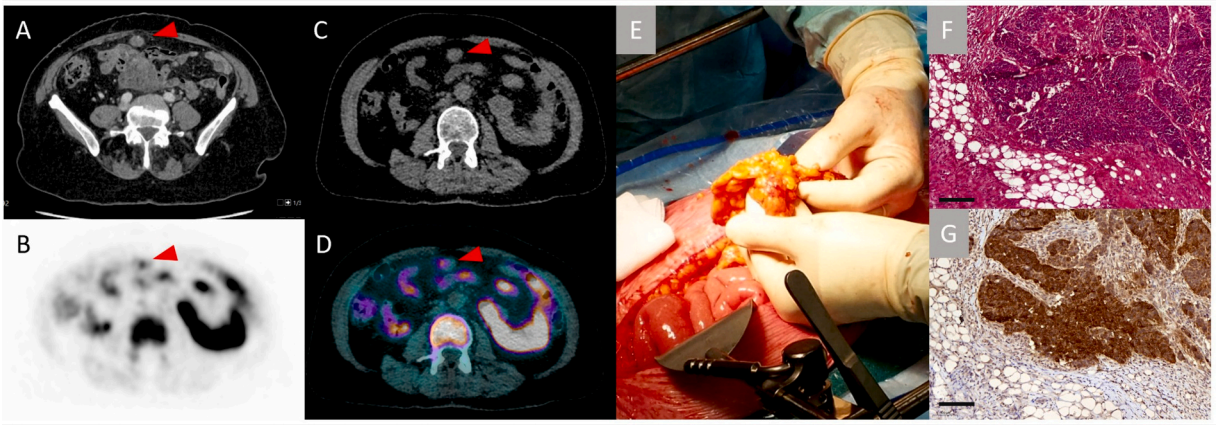

Fig. 2. A metastatic EOC lesion in the central region correlated on diagnostic CT image, on [^{18}F]fluoro-PEG-folate PET/CT image, during surgery, on microscopic images (HE staining) and with immunohistochemical staining. A metastatic lesion of approximately 2 cm in the central region, indicated by red/blue arrow on **(A)** axial contrast-enhanced CT image; **(B–D)** axial [^{18}F]fluoro-PEG-folate on PET/CT images. Note that the lesion showed high uptake centrally and some mismatch in fusion images due to bowel displacement; **(E)** photograph during surgery. **(F)** Microscopic detail (H&E staining; **(G)** IHC staining for FRα). Scale bars in (F) and (G) represent 200 μm.

associated FRα. They did, however, show a strong positive staining for FRβ, which is expressed in activated macrophages present in lymph nodes (Fig. 3).

4. Discussion

This first-in-human study in patients with advanced EOC suggests that, although [^{18}F]fluoro-PEG-folate was safe to use, its efficacy in terms of tumor-specific imaging and detecting the extent of disease was limited in EOC. The study was terminated prematurely during the interim analysis after five out of 15 scheduled participants had completed the study protocol, due to unsatisfactory results regarding feasibility.

In the five patients who underwent the [^{18}F]fluoro-PEG-folate PET/CT scan, no serious adverse events (SAEs) were documented, and there were no relevant changes in vital function parameters, providing further evidence of the safety profile of [^{18}F]fluoro-PEG-folate [27]. However, despite clear FRα overexpression observed by immunohistochemistry (Table 3), we noted low [^{18}F]fluoro-PEG-folate tracer uptake in all histologically proven malignant EOC lesions. Conversely, as observed in Verweij et al.'s study with [^{18}F]fluoro-PEG-folate [27], we observed high tracer uptake in various healthy tissues including the liver, spleen, bone marrow, biliary system, stomach, duodenum, pancreas, adrenal glands, renal cortices, renal pelvis, ureters, bowel, and lymph nodes. Particularly due to the high uptake in the liver, spleen and bowel, it is unlikely that the tracer will improve the detection of lesions located in the areas that are most difficult to diagnose with contrast-enhanced CT, namely, the spaces beneath the diaphragm, peritoneal carcinomatosis on the serosa and mesentery of the bowel. As previously shown in animal studies, [^{18}F]fluoro-PEG-folate binds to all isoforms of folate including FRβ [31], which is naturally present in the organs exhibiting tracer uptake in this study. This suggests that while FRα may predominate in EOC tissue, FRβ could be more prominent in healthy tissues, potentially leading to preferential uptake of [^{18}F]fluoro-PEG-folate in these organs [32]. Moreover, the presence of tracer in the gastrointestinal tract can be attributed to the involvement of folate receptors in the absorption of dietary folate. As a result, the tracer may bind to these receptors as part of the regular physiological process of clearance [33].

Additionally, the tumor microenvironment, characterized by factors such as hypoxia, acidity, and elevated interstitial fluid pressure, could significantly influence tracer distribution and retention within tumor tissue, potentially diminishing its uptake [34]. Four out of five patients received NACT, which can cause structural changes to the tumor such as fibrosis and calcifications, further negatively impacting tracer uptake. Although 47 lymph nodes across all five patients were positive on [^{18}F]fluoro-PEG-folate PET/CT images, they were not considered suspicious for malignancy during surgery. Only one conglomerate of three lymph nodes, which initially appeared suspicious on PET/CT, was excised during surgery. However, pathology results showed tumor negative lymph nodes. This discrepancy could be explained by the expression of FRβ in activated macrophages found in lymph nodes, as reported in previous studies [22,23], and confirmed in this study (Fig. 3). This suggests a lack of specificity of [^{18}F]fluoro-PEG-folate PET for EOC lesions.

In contrast to the findings by Verweij et al. where the activity in the descending aorta reached zero following the arterial peak [27], we observed residual activity in this region. A reason for this discrepancy could be that platinum-based chemotherapy directly causes vascular endothelial cell dysfunction as platinum compounds induce endothelial cell damage. This damage can trigger the recruitment of macrophages as part of the inflammatory response [35]. Since macrophages express FRβ, this can lead to a slight increase in tracer uptake in vessel walls. Earlier

Table 2
Display of PCI scores on [^{18}F]fluoro-PEG-folate PET/CT images ($PCI_{PET/CT}$) and during surgery at initial ($PCI_{surgery1}$) and secondary ($PCI_{surgery2}$) exploration, and histopathologic results.

Patient	PCI	0 (central)	1 (right upper)	2 (epigastrium)	3 (left upper)	4 (left flank)	5 (left lower)	6 (pelvis)	7 (right lower)	8 (right flank)	9 (upper jejunum)	10 (lower jejunum)	11 (upper ileum)	12 (lower ileum)	Total
1	$PCI_{PET/CT}$	1	0	0	0	1	1	2	2	1	1	1	0	1	**11**
	$PCI_{surgery1}$	2	0	0	0	0	0	2	1	1	0	0	1	1	**8**
	$PCI_{surgery2}$	2	0	0	0	0	0	2	2	1	0	0	1	1	**9**
	Histology	pos	-	-	-	-	-	pos	pos	pos	-	-	m	m	n/a
2	$PCI_{PET/CT}$	0	0	0	0	1	2	3	0	1	1	1	1	3	**13**
	$PCI_{surgery1}$	0	0	0	0	1	0	3	3	1	1	1	1	1	**12**
	$PCI_{surgery2}$	0	0	0	0	1	0	3	3	1	1	1	1	1	**12**
	Histology	pos	-	-	-	pos	-	pos	pos	m	m	m	m	pos	n/a
3	$PCI_{PET/CT}$	3	0	3	0	0	0	0	0	0	1	0	1	0	**8**
	$PCI_{surgery1}$	3	0	3	0	0	0	0	1	0	0	0	0	0	**7**
	$PCI_{surgery2}$	3	0	3	0	0	0	0	1	0	0	0	0	0	**7**
	Histology	pos	-	pos	-	-	-	pos	neg	-	-	-	-	-	n/a
4	$PCI_{PET/CT}$	3	0	0	0	0	1	0	1	0	0	0	0	0	**5**
	$PCI_{surgery1}$	0	0	0	0	0	0	1	0	1	0	0	0	0	**2**
	$PCI_{surgery2}$	2	0	0	0	0	0	1	0	1	0	0	0	0	**4**
	Histology	pos	-	-	-	-	-	pos	-	pos	-	-	-	-	n/a
5	$PCI_{PET/CT}$	2	0	0	0	0	0	3	0	3	0	0	0	0	**8**
	$PCI_{surgery1}$	2	0	0	0	0	0	3	0	0	0	0	0	0	**5**
	$PCI_{surgery2}$	2	0	0	0	0	0	3	0	1	0	0	0	0	**6**
	Histology	pos	-	-	-	-	-	pos	-	pos	-	-	-	-	n/a

PCI scores are depicted for each region based on the amount of tumor involvement: 0 for no macroscopic tumor, 1 for small (<0.5 cm), 2 for moderate (0.5–5.0 cm) and 3 for large tumor lesions (>5 cm) [29] and summed up in the last column for each of the methods used (PET/CT, surgery at initial exploration and surgery at secondary exploration). The abbreviations used indicate the following: "-"; non-applicable (no histopathologic sample because of non-malignant appearance during surgery). "m"; missing (no histopathologic sample despite macroscopically malignant appearance, because biopsies were already taken from similar lesions in a different region). "pos"; tumor positive. "neg"; tumor negative on histopathology.

Table 3
Total immunostaining score (TIS) of the tumor-positive resected lesions immunohistochemically stained for FRα.

Biomarker	Primary CRS		NACT/Interval CRS	
	No overexpression (TIS 0–4)	Overexpression (TIS 6–12)	No overexpression (TIS 0–4)	Overexpression (TIS 6–12)
FRα (33)	0 (0 %)	10 (100 %)	1 (4 %)	22 (96 %)

we described the pharmacokinetic properties of the tracer and observed variations in plasma concentrations of radioactive folate among patients, as well as differences in relative tracer uptake [28]. Competitive binding with native folate could potentially account for these variations. The one-week restriction on folate supplements in our study could have been superfluous as dietary folate intake may also influence folate plasma concentrations over a longer period. Extending the supplement restriction, however, was not feasible as it would require an undesirable delay of imaging and surgery after inclusion.

Overall, we observed slightly higher $PCI_{PET/CT}$ scores compared to $PCI_{surgery2}$ scores, albeit with a difference of 1–2 points. However, recognizing metastatic lesions solely from the PET image proved to be challenging without reviewing the low dose CT images and previously acquired contrast-enhanced CT images. An additional complicating factor was the mismatch that occurred in all scans due to bowel movement and bladder filling. Notably, across all five patients, three additional small tumor lesions (in two different patients), not recognized by initial surgical exploration, were removed based on additional information provided by the PET/CT images. On the other hand, in five regions in three patients, proven malignant lesions were missed on PET/CT images.

Furthermore, evaluating the extent of disease by using the PCI scores per region is arguable, as only the largest lesions per region are typically considered in the PCI scoring system, masking the potential impact of smaller lesions on the comparison of tumor load (i.e., a region can contain a smaller falsely predicted lesion as well as a correctly predicted larger lesion). Moreover, the PCI scoring system is subject to inherent subjectivity and interobserver variability, which can introduce

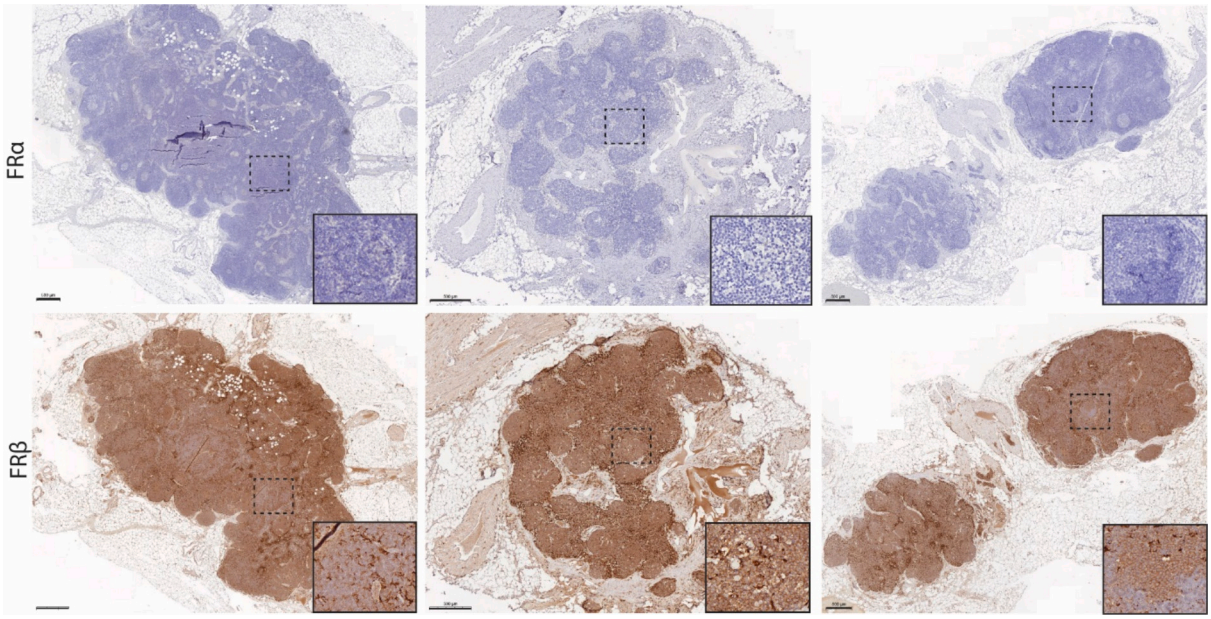

Fig. 3. Images of immunohistochemical staining of a conglomerate of three false-positive lymph nodes on PET/CT images. The top row shows an absence of FRα in these lymph nodes, while the bottom row shows the same lymph nodes with strong positive staining for FRβ. Scale bars represent 500 μm. Inserts were taken at 22.4× magnification.

inconsistencies and inaccuracies into the assessment process, potentially influencing the comparison of tumor burden between patients or studies [36,37].

A limitation of the study is that histopathological data from several PET-positive lesions were unavailable because samples were not collected from clinically unsuspected lesions according to the protocol as advised by the Medical Ethics Committee. Consequently, we could not evaluate the diagnostic accuracy of [^{18}F]fluoro-PEG-folate PET/CT in detecting malignant EOC lesions. Another limitation of this study is the small sample size, although it is inherent to the proof-of-concept character of the study. However, given the consistent pattern of low tracer uptake in tumor tissue and high uptake in healthy tissue, it is questionable whether a larger cohort will yield different results. The tracer showed a low target-to-background ratio and low tumor specificity due to its accumulation in normal lymph nodes and various healthy tissues expressing FRβ. Additionally, the lack of multimodal benefits from CT, caused by mismatches from bowel movements and bladder filling, further limits its effectiveness. Consequently, it appears unlikely that [^{18}F]fluoro-PEG-folate PET/CT will have a promising future for pre-operative imaging of metastatic EOC.

In conclusion, [^{18}F]fluoro-PEG-folate is a well-tolerated radiotracer. Our findings, however, suggest that [^{18}F]fluoro-PEG-folate PET/CT does not provide added value in the pre-operative assessment of intra-abdominal metastatic tumor burden in patients with advanced stage EOC. Moving forward, it is imperative to prioritize further research aimed at identifying novel imaging agents tailored to specifically target EOC while exhibiting minimal expression in healthy tissues, thus enhancing both imaging and therapeutic applications.

Ethical approval

This study was performed in line with the principles of the 1964 Helsinki Declaration and its later amendments or comparable ethical standards. Approval was granted by the Medical Ethics Committee Leiden-Den Haag-Delft (protocol P20.048) in 2021.

Funding

This study was supported by the Bontius Stichting, a Leiden University Medical Center Research Foundation.

CRediT authorship contribution statement

Isabeau A. Ciggaar: Writing – review & editing, Writing – original draft, Visualization, Validation, Project administration, Investigation, Formal analysis. **Lysanne D.A.N. de Muynck:** Writing – review & editing, Writing – original draft, Visualization, Investigation, Formal analysis. **Lioe-Fee de Geus-Oei:** Writing – review & editing, Writing – original draft, Validation, Supervision, Resources, Methodology, Investigation, Formal analysis, Conceptualization. **Floris H.P. van Velden:** Writing – review & editing, Writing – original draft, Methodology, Investigation, Formal analysis, Conceptualization. **Cornelis D. de Kroon:** Writing – review & editing, Writing – original draft, Investigation. **Lenka M. Pereira Arias-Bouda:** Writing – review & editing, Writing – original draft, Investigation. **Wyanne A. Noortman:** Writing – review & editing, Writing – original draft, Investigation. **Els L. van Persijn van Meerten:** Writing – review & editing, Writing – original draft, Investigation. **Petra Dibbets-Schneider:** Writing – review & editing, Writing – original draft, Investigation. **Hendrik J.F. Helmerhorst:** Writing – review & editing, Writing – original draft, Investigation. **Albert D. Windhorst:** Writing – review & editing, Writing – original draft, Investigation. **Alexander L. Vahrmeijer:** Writing – review & editing, Writing – original draft, Investigation. **Inge T.A. Peters:** Writing – review & editing, Writing – original draft, Visualization, Supervision, Resources, Methodology, Investigation, Funding acquisition, Conceptualization. **Katja N. Gaarenstroom:** Writing – review & editing, Writing – original draft, Visualization, Validation, Supervision, Resources, Project administration, Methodology, Investigation, Funding acquisition, Formal analysis, Conceptualization.

Declaration of competing interest

A.D. Windhorst is editor-in-chief of Nuclear Medicine & Biology and was not involved in the editorial review or the decision to publish this article. All other authors have no relevant financial or non-financial interests to disclose.

Acknowledgements

The authors would like to thank the following co-workers for their involvement in the study protocol, patient care and/or conducting study activities: T. Bosse, pathologist; J.J. Beltman and L.S. Nooij, gynecologic oncologists; N. Bouwman, clinical pharmacist; and J. Kuil, medical physicist.

Appendix A. Supplementary data

Supplementary data to this article can be found online at https://doi.org/10.1016/j.nucmedbio.2024.108952.

References

[1] Berek JS, Renz M, Kehoe S, Kumar L, Friedlander M. Cancer of the ovary, fallopian tube, and peritoneum: 2021 update. Int J Gynaecol Obstet 2021;155(Suppl. 1):61–85.
[2] Ledermann JA, Matias-Guiu X, Amant F, Concin N, Davidson B, Fotopoulou C, et al. ESGO-ESMO-ESP consensus conference recommendations on ovarian cancer: pathology and molecular biology and early, advanced and recurrent disease. Ann Oncol 2024;35:248–66.
[3] Peters ITA, Marchetti C, De Palma A, Giannarelli D, Carcagnì A, Scambia G, et al. Cytoreductive surgery for advanced epithelial ovarian cancer in the poly(ADP-ribose) polymerase inhibitors era-is it time for a new paradigm shift? A systematic review and meta-analysis. Eur J Cancer 2023;187:77–86.
[4] Vergote I, Coens C, Nankivell M, Kristensen GB, Parmar MKB, Ehlen T, et al. Neoadjuvant chemotherapy versus debulking surgery in advanced tubo-ovarian cancers: pooled analysis of individual patient data from the EORTC 55971 and CHORUS trials. Lancet Oncol 2018;19:1680–7.
[5] Nougaret S, Sadowski E, Lakhman Y, Rousset P, Lahaye M, Worley M, et al. The BUMPy road of peritoneal metastases in ovarian cancer. Diagn Interv Imaging 2022;103:448–59.
[6] van't Sant I, Engbersen MP, Bhairosing PA, DMJ Lambregts, RGH Beets-Tan, van Driel WJ, et al. Diagnostic performance of imaging for the detection of peritoneal metastases: a meta-analysis. Eur Radiol 2020;30:3101–12.
[7] Heitz F, Harter P, Alesina PF, Walz MK, Lorenz D, Groeben H, et al. Pattern of and reason for postoperative residual disease in patients with advanced ovarian cancer following upfront radical debulking surgery. Gynecol Oncol 2016;141:264–70.
[8] Grabowski JP, Harter P, Heitz F, Pujade-Lauraine E, Reuss A, Kristensen G, et al. Operability and chemotherapy responsiveness in advanced low-grade serous ovarian cancer. An analysis of the AGO Study Group metadatabase. Gynecol Oncol 2016;140:457–62.
[9] Fagotti A, Ferrandina G, Fanfani F, Ercoli A, Lorusso D, Rossi M, et al. A laparoscopy-based score to predict surgical outcome in patients with advanced ovarian carcinoma: a pilot study. Ann Surg Oncol 2006;13:1156–61.
[10] Petrillo M, Vizzielli G, Fanfani F, Gallotta V, Cosentino F, Chiantera V, et al. Definition of a dynamic laparoscopic model for the prediction of incomplete cytoreduction in advanced epithelial ovarian cancer: proof of a concept. Gynecol Oncol 2015;139:5–9.
[11] Rutten MJ, van Meurs HS, van de Vrie R, Gaarenstroom KN, Naaktgeboren CA, van Gorp T, et al. Laparoscopy to predict the result of primary cytoreductive surgery in patients with advanced ovarian cancer: a randomized controlled trial. J Clin Oncol 2017;35:613–21.
[12] van de Vrie R, Rutten MJ, Asseler JD, Leeflang MM, Kenter GG, Mol BWJ, et al. Laparoscopy for diagnosing resectability of disease in women with advanced ovarian cancer. Cochrane Database Syst Rev 2019;(3):Cd009786.
[13] Gueli Alletti S, Capozzi VA, Rosati A, De Blasis I, Cianci S, Vizzielli G, et al. Laparoscopy vs. laparotomy for advanced ovarian cancer: a systematic review of the literature. Minerva Med 2019;110:341–57.
[14] Michielsen K, Dresen R, Vanslembrouck R, De Keyzer F, Amant F, Mussen E, et al. Diagnostic value of whole body diffusion-weighted MRI compared to computed tomography for pre-operative assessment of patients suspected for ovarian cancer. Eur J Cancer 2017;83:88–98.
[15] Dumont S, Vandecaveye V, Dresen RC, Van Nieuwenhuysen E, Baert T, Amant F, et al. Predicting resectable disease in relapsed epithelial ovarian cancer by using whole-body diffusion-weighted MRI. Int J Gynecol Cancer 2023;33:1890–7.
[16] Dezen T, Rossini RR, Spadin MD, Da Cunha Andrade CEM, Schimidt R, Vieira MA, et al. Accuracy of MRI for diagnosing pelvic and para-aortic lymph node metastasis in cervical cancer. Oncol Rep 2021;45:100.
[17] Mieog JSD, Achterberg FB, Zlitni A, Hutteman M, Burggraaf J, Swijnenburg RJ, et al. Fundamentals and developments in fluorescence-guided cancer surgery. Nat Rev Clin Oncol 2022;19:9–22.
[18] Crane LM, Arts HJ, van Oosten M, Low PS, van der Zee AG, van Dam GM, et al. The effect of chemotherapy on expression of folate receptor-alpha in ovarian cancer. Cell Oncol (Dordr) 2012;35:9–18.
[19] Despierre E, Lambrechts S, Leunen K, Berteloot P, Neven P, Amant F, et al. Folate receptor alpha (FRA) expression remains unchanged in epithelial ovarian and endometrial cancer after chemotherapy. Gynecol Oncol 2013;130:192–9.
[20] Muynck L, Gaarenstroom KN, Sier CFM, Duijvenvoorde MV, Bosse T, Mieog JSD, et al. Novel molecular targets for tumor-specific imaging of epithelial ovarian cancer metastases. Cancers (Basel) 2020:12.
[21] Vergote IB, Marth C, Coleman RL. Role of the folate receptor in ovarian cancer treatment: evidence, mechanism, and clinical implications. Cancer Metastasis Rev 2015;34:41–52.
[22] Randall LM, Wenham RM, Low PS, Dowdy SC, Tanyi JL. A phase II, multicenter, open-label trial of OTL38 injection for the intra-operative imaging of folate receptor-alpha positive ovarian cancer. Gynecol Oncol 2019;155:63–8.
[23] Hoogstins CES, Tummers QRJG, Gaarenstroom KN, de Kroon CD, Trimbos JBMZ, Bosse T, et al. A novel tumor-specific agent for intraoperative near-infrared fluorescence imaging: a translational study in healthy volunteers and patients with ovarian cancer. Clin Cancer Res 2016;22:2929–38.
[24] Ocak M, Gillman AG, Bresee J, Zhang L, Vlad AM, Muller C, et al. Folate receptor-targeted multimodality imaging of ovarian cancer in a novel syngeneic mouse model. Mol Pharm 2015;12:542–53.
[25] Brand C, Longo VA, Groaning M, Weber WA, Reiner T. Development of a new folate-derived Ga-68-based PET imaging agent. Mol Imaging Biol 2017;19:754–61.
[26] Chen Q, Meng X, McQuade P, Rubins D, Lin SA, Zeng Z, et al. Synthesis and preclinical evaluation of folate-NOTA-Al(18)F for PET imaging of folate-receptor-positive tumors. Mol Pharm 2016;13:1520–7.
[27] Verweij NJF, Yaqub M, Bruijnen STG, Pieplenbosch S, ter Wee MM, Jansen G, et al. First in man study of [18F]fluoro-PEG-folate PET: a novel macrophage imaging technique to visualize rheumatoid arthritis. Sci Rep 2020;10:1047.
[28] Ruytenberg T, Ciggaar IA, Peters ITA, Noortman WA, Dibbets-Schneider P, de Muynck LDAN, et al. Challenges in pharmacokinetic modelling of [18F]fluoro-PEG-folate PET/CT imaging in epithelial ovarian cancer patients. Mol Imaging Biol 2024;26(4):577–84.
[29] Jacquet P, Sugarbaker PH. Clinical research methodologies in diagnosis and staging of patients with peritoneal carcinomatosis. Cancer Treat Res 1996;82:359–74.
[30] van Driel WJ, Koole SN, Sikorska K, Schagen van Leeuwen JH, Schreuder HWR, Hermans RHM, et al. Hyperthermic intraperitoneal chemotherapy in ovarian cancer. N Engl J Med 2018;378:230–40.
[31] Gent YY, Weijers K, Molthoff CF, Windhorst AD, Huisman MC, Smith DE, et al. Evaluation of the novel folate receptor ligand [18F]fluoro-PEG-folate for macrophage targeting in a rat model of arthritis. Arthritis Res Ther 2013;15:R37.
[32] Wallace-Povirk A, Hou Z, Nayeen MJ, Gangjee A, Matherly LH. Folate transport and one-carbon metabolism in targeted therapies of epithelial ovarian cancer. Cancers 2022;14:191.
[33] Frigerio B, Bizzoni C, Jansen G, Leamon CP, Peters GJ, Low PS, et al. Folate receptors and transporters: biological role and diagnostic/therapeutic targets in cancer and other diseases. J Exp Clin Cancer Res 2019;38:125.
[34] Abadjian M-CZ, Edwards WB, Anderson CJ. Imaging the tumor microenvironment. In: Kalinski P, editor. Tumor immune microenvironment in cancer progression and cancer therapy. Cham: Springer International Publishing; 2017. p. 229–57.
[35] Hsu P-Y, Mammadova A, Benkirane-Jessel N, Désaubry L, Nebigil CG. Updates on anticancer therapy-mediated vascular toxicity and new horizons in therapeutic strategies. Front Cardiovasc Med 2021:8.
[36] Gouy S, Belghiti J, Uzan C, Canlorbe G, Gauthier T, Morice P. Accuracy and reproducibility of the peritoneal cancer index in advanced ovarian cancer during laparoscopy and laparotomy. Int J Gynecol Cancer 2013:23.
[37] Bhatt A, Yonemura Y, Mehta S, Benzerdjeb N, Kammar P, Parikh L, et al. The pathologic peritoneal cancer index (PCI) strongly differs from the surgical PCI in peritoneal metastases arising from various primary tumors. Ann Surg Oncol 2020;27:2985–96.